



Microstructure Evolution of Ultra-Fine-Grained AZ31 B Magnesium Alloy Produced by Submerged Friction Stir Processing

Ali Shahnam, Fathallah Karimzadeh, Mohammad Ali Golozar, and Seyedeh Narjes Hosseini

(Submitted August 20, 2018; in revised form May 6, 2019; published online July 15, 2019)

Ten-millimeter-thick strain-hardened AZ31B-H24 magnesium sheets were subjected to friction stir processing (FSP) in air and submerged friction stir processing (SFSP) under water to investigate their microstructures and microhardness properties. Different rotational speeds of 500, 630, 800, and 1000 rpm and traverse speeds of 50, 100, 200, and 350 mm/min were employed for processing the materials. For SFSPed samples, the rotational speed of 500 rpm and 200 mm/min of traverse speed resulted in an ultra-fine-grained structure with a minimum grain size of about 400–500 nm, which is half compared to that of FSPed. It was found that both processes led to variation of crystallographic orientation, and enhancing the rotational speed and lowering the traverse speed promoted the development of a {0002} basal texture. The microhardness of SFSPed material increased significantly up to 110% (~ 95 Hv), while the microhardness was 45% (~ 65 Hv) higher than the base metal (~ 45 Hv) for FSPed material.

Keywords AZ31 B magnesium alloy, microhardness
microstructure, nonferrous metals, texture, welding

1. Introduction

Magnesium alloys are considered as a lucrative option in the transportation industry due to their low density, high strength-to-weight ratio, castability, environmental friendliness, and recyclability. As welding and joining are inevitably part of the manufacturing process of structural materials, understanding the weldability of these alloys is essential (Ref 1). Also, the microstructural modifications such as grain size refinement have proved to be an effective strategy for enhancing the mechanical properties of magnesium alloys. Friction stir processing (FSP) is an attractive and green solid-state joining technique to produce fine grain structures via severe plastic deformation and repeated dynamic recrystallization, which also significantly mitigate the challenges usually induced by fusion welding of magnesium alloys such as hot cracking, segregation or precipitation of undesirable particles (Ref 1–6). Recently, successful FSP of Mg-based alloys for producing ultra-fine grained (UFG) structures (less than 1–5 μm) have been widely reported (Ref 7–12). Taking into account that thermal cycles associated with FSP may cause rapidly grain growth and coarsening of the structure, fluid cooling with water or liquid nitrogen during the submerged friction stir processing (SFSP)

seems to be very useful to improve the mechanical properties by controlling the thermal cycling (Ref 13–16).

There are many investigations on SFSP of Al alloys, concerning the improvement of mechanical properties by grain size refinement (Ref 17–19). However, only very few studies have been reported on SFSP of Mg alloys. Mofid et al. (Ref 20) showed that SFSP of AA5083/Mg AZ31 alloys, underwater, and under liquid nitrogen, significantly suppressed the formation of intermetallic compounds contributed to cracking in the weld nugget. Darras et al. (Ref 21) and Chai et al. (Ref 22) reported that SFSP of AZ31 B-O and AZ91 Magnesium alloys led to significant grain refinement, porosity reduction, and formability enhancement.

In this paper, the effects of different operation conditions on the microstructures and microhardness of the FSPed and SFSPed AZ31 magnesium sheets were investigated.

2. Experimental Procedure

2.1 Materials

The base metal was a strain-hardened and partially annealed AZ31B-H24 magnesium alloy sheet with a hardness of 45 Hv. Figure 1 shows the microstructure of the AZ31B-H24 alloy. Table 1 gives the chemical composition of the samples. The FSP and SFSP specimens had the dimensions of $10 \times 50 \times 250 \text{ mm}^3$.

2.2 FSP and SFSP Procedure

The FSP and SFSP machines used in the present study were modified mills with a vertical head. A nonconsumable tool with a 4-mm pin swept diameter was made of H13 tool steel. To improve wear resistance and strength of the FSP tool, the following heat treatment cycle was applied: (1) austenitization at 1050 °C for 1 h, (2) water quenching to room temperature, and (3) tempering at 450 °C for 20 min (Ref 4). This led to

Ali Shahnam, Fathallah Karimzadeh, and Mohammad Ali Golozar, Department of Materials Engineering, Isfahan University of Technology, Esfahan 84156-83111, Iran; Seyedeh Narjes Hosseini, Department of Mechanical Engineering, Persian Gulf University, Bushehr 75169-13798, Iran. Contact e-mails: f_karimzadeh@cc.iut.ac.ir, n.hosseini@pgu.ac.ir, and narjeshosseini@gmail.com.

increasing the hardness of the tool steel from 48 to 63 HRC after this procedure. Different rotational (500, 630, 800, and 1000 rpm) and traverse (50, 100, 200, and 350 mm/min) speeds were the processing parameters employed. The temperature measurement carried out using an embedded K-type thermocouple. The SFSP process performed under water, as shown in Fig. 2.

2.3 Materials Characterization

Samples microstructures were investigated using optical microscopy (OM), scanning electron microscopy (SEM, Philips XL30), and transmission electron microscopy (TEM, Tecnai F30). All the samples were taken from the transverse section of the processed area at the middle of the sheet thickness. Picraletchant (Ref 5) (consisting of 0.4 g picric acid, 13 mL ethanol, 3 mL glacial acetic acid, and 3 mL boiled water) was used to prepare the specimens for microstructural studies. Texture of FSPed and SFSPed AZ31 magnesium alloys were analyzed for the normal direction sections [rolling direction (RD) and longitudinal direction (TD)]. Three pole figures, $\{0002\}$, $\{10\bar{1}0\}$, and $\{10\bar{1}1\}$, were measured by x-ray diffraction (XRD, D8 Discover) with Cu $K\alpha$ radiation (40 kV, 200 mA, tilt angle of 0-85°). Microhardness profiles of the FSP and SFSP specimens were measured on the cross sections perpendicular to the processing direction, using a Vickers indenter with a 100-gf load for 30 s.

3. Results and Discussion

3.1 Microstructural Features

Figure 3 shows the microstructure of different regions after friction stir process with rotational and traverse speeds of 630 rpm and 200 mm/min, respectively. As-received AZ31B-H24 magnesium alloy consisted of a single-phase coarse-grain structure ($\sim 75 \pm 6 \mu\text{m}$ —Fig. 1). However, in the FSPed

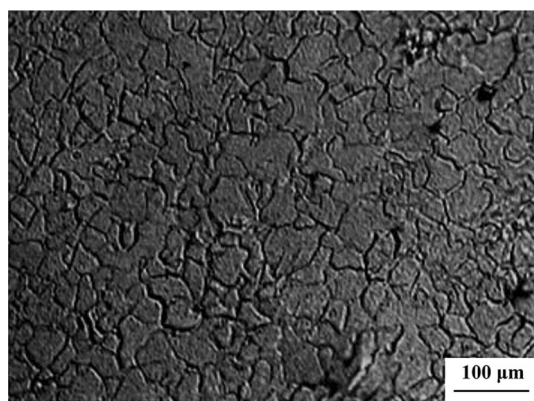


Fig. 1 Microstructure of the AZ31B-H24 base metal

sample, two different microstructural zones, stirred zone (SZ) and thermo-mechanical affected zone (TMAZ), have significantly lower grain sizes (Fig. 3a). This can be attributed to the high plastic deformation and dynamic recrystallization that occur during the FSP process (Ref 23).

The grain size values in TMAZ region is approximately $3 \pm 0.7 \mu\text{m}$ (Fig. 3b), while this decrease is more obvious in the SZ with a basin shape and fine recrystallized grains. The stir zone can be divided into two sub-zones: SZI and SZII. SZI, located at the upper center of stirred zone, is characterized by partially dynamically recrystallized and deformed grains. The average grains size in this sub-zone is approximately $2 \pm 0.5 \mu\text{m}$ (Fig. 3c). In SZII subregion, located under the tool pin, full dynamic recrystallization is occurred, resulting in an average grain size of approximately $950 \pm 45 \text{ nm}$ (Fig. 3d). It should be noted that the heat affected zone was not obvious because of the existence of a single-phase microstructure.

Figure 4(a) shows the sharp interface between stir zone and TMAZ in SFSP sample. In this sample, the tool shoulder is surrounded by water, so the stirred sample temperature can quickly reduce during and after the process. Thus, heat is more localized around the tool.

Temperature analyses illustrated in Fig. 5 confirm that the lower peak temperature and the lower duration at peak temperature in SFSP in comparison with FSP resulted in additional refinement of grain size in the submerged samples.

This can be explained by Eq 1 which describes the relation between recrystallized grains size and temperature (Ref 6):

$$D^2 - D_0^2 = At^n \exp\left(-\frac{Q}{RT}\right) \quad (\text{Eq 1})$$

where D and D_0 are, respectively, recrystallized and primary grains sizes; t is the time of grain growth; R is ideal gas constant; Q is the activation energy and n and A are constant values related to composition and temperature which are

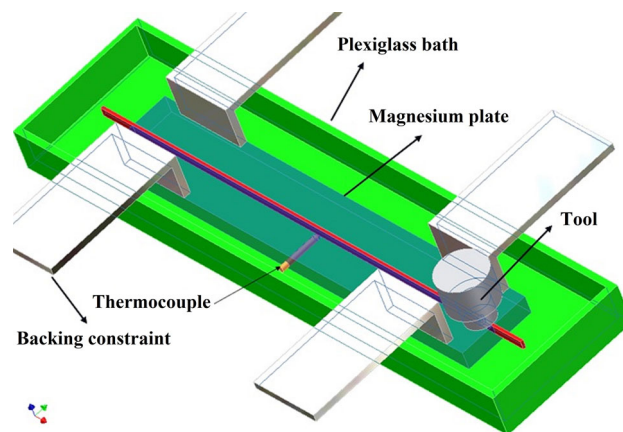


Fig. 2 Schematic representation of apparatus set up used for SFSP

Table 1 Chemical composition of Mg AZ 31B alloy

Element	Al	Zn	Mn	Si	Fe	Cu	Ni	Mg
Weight percent	2.5-3.5	0.6-1.4	0.2-1.0	0.1	0.005	0.04	0.005	Bal

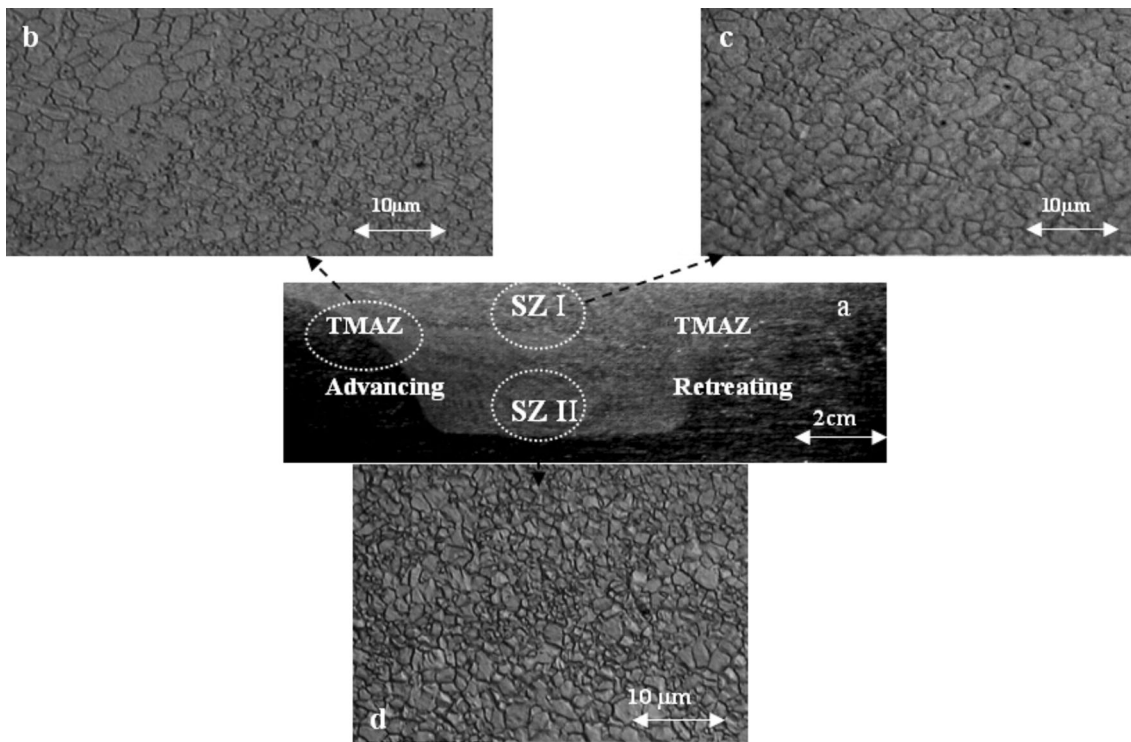


Fig. 3 Typical stir zone, TMAZ and BM microstructure of FSP Mg-AZ31 B alloy processed at $\omega = 630$ rpm, $V = 200$ mm/min: (a) enlarged micrograph of the stir zone, TMAZ, and BM; (b) microstructure of the TMAZ/SZ II interface; (c) microstructure of the SZ I; (d) microstructure of the SZ II

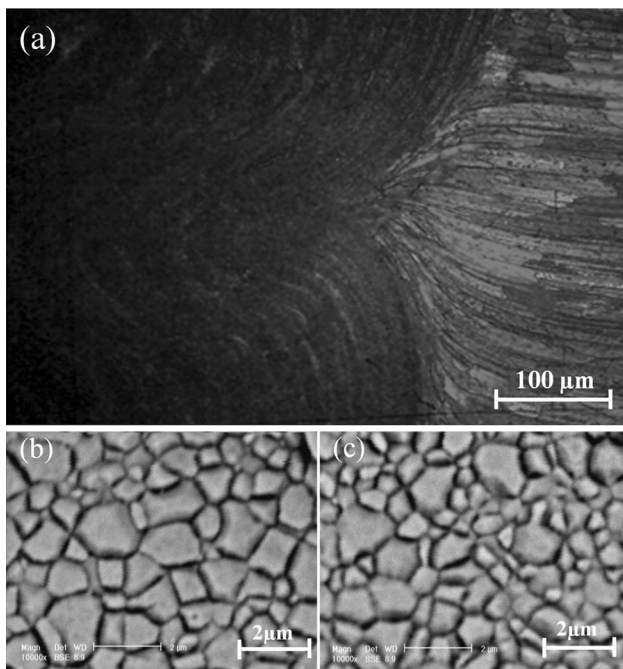


Fig. 4 (a) Optical microscopy of SFSP sample ($\omega = 630$ rpm, $v = 200$ mm/min), SEM micrographs of (b) FSP and (c) SFSP samples ($\omega = 500$ rpm, $v = 50$ mm/min)

independent of grains sizes. According to this equation grains sizes decrease when the maximum temperature of friction zone reduces. This situation is visible in Fig. 4(b) and (c) which show SEM micrographs of stir zones in FSP and SFSP samples

in constant rotational and traverse speeds. The grain size of FSP sample was approximately $1 \pm 0.5 \mu\text{m}$, while this value decreased to 800 ± 100 nm in SFSP sample.

3.1.1 Grain Refinement Mechanism in FSP/SFSP. Nucleation of equiaxed dislocation-free new grains due to dynamic recrystallization owing to an intensive plastic deformation leads to fine grain structure in the stir zone (Ref 14).

Bright-field TEM micrographs in Fig. 6 reflects the boundaries disorientation indicating the generation of low-angle boundaries (LABs)— 2° - 15° —within the larger persistent grains, and also the dislocation rearrangement in the process of refining these grains. The size of sub-grains is decreased gradually, and the percentage of LABs is increased with increasing traverse speed. Fine grains gradually develop misorientations to produce high-angle boundaries (HABs) and the recrystallized grains eventually cease to grow. The obvious nucleation and growth stages suggest that this microstructural evolution can be classified as discontinuous dynamic recrystallization (DDR_X).

3.2 Effects of Process Parameters on the Temperature Profile

From Fig. 7, it is clear that the size of equiaxed grains in the stir zone was decreased with decreasing rotation speed and increasing traverse speed.

The recrystallization grain size can be reduced by slower rotational and higher traverse speeds. In fact, higher rotation rate or greater tool rotation rate/traverse speed proportion causes increasing both deformation degree and peak temperature. The first results in reducing recrystallized grain size (see Eq 1) the latter leads to the generation of coarse grains during recrystallization, and also grain growth (Ref 24).

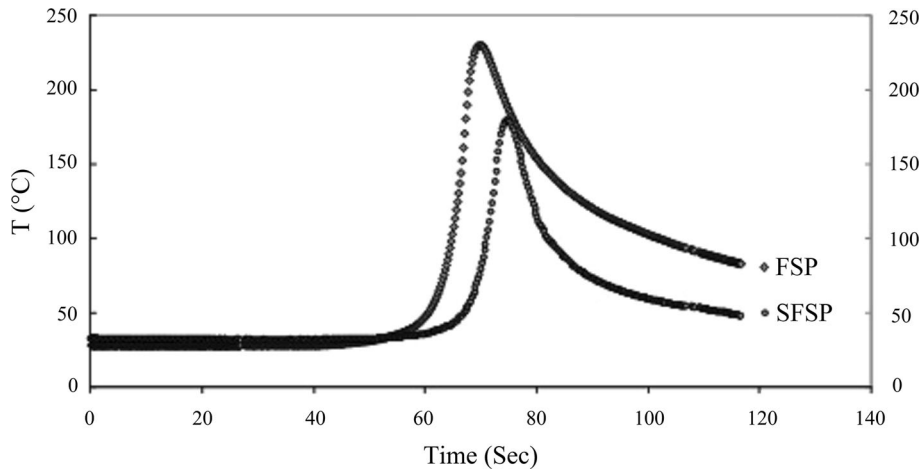


Fig. 5 The temperature profile in FSP and SFSP samples ($\omega = 500$ rpm, $V = 200$ mm/min)

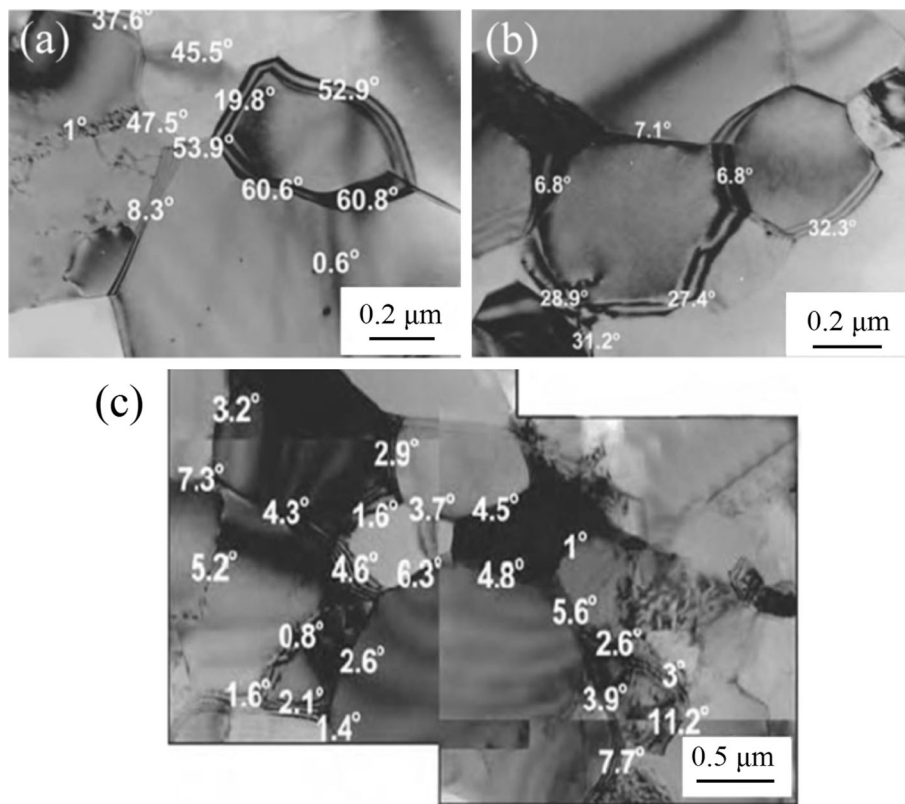


Fig. 6 Bright-field TEM micrographs showing the DRX microstructure at various traverse speed (a) 50 mm/min (b) 200 mm/min and (c) 350 mm/min at rpm of 500

Heat index ($w = \omega^2/\nu$) was introduced as a parameter to evaluate the effect of rotation and traverse speeds on temperature produced during the friction process, as below (Ref 2):

$$\frac{T}{T_m} = K \left(\frac{\omega^2}{V \times 10^4} \right)^\alpha = K \delta^\alpha \quad (\text{Eq 2})$$

where ω and V are rotation and traverse speeds, T and T_m are peak temperature and melting temperature, respectively; α exponent and K are constant values dependant on materials characteristics and heat conductivity.

Variation of temperature with heat index for FSPed and SFSPed samples is shown in Fig. 8(a). As expected, the temperature of stir zone was raised by increasing the heat index in both processes. Figure 8(b) shows the change of T/T_m with the heat index. The constant values in Eq 2 for the current alloy in FSP and SFSP processes can be obtained from these curves. So, Eq 2 is rewritten in the form of Eq 3 and 4 for FSPed and SFSPed AZ31 B magnesium alloy, respectively ($T_m \sim 650^\circ\text{C}$). Lower K value in SFSPed sample emphasizes the more heat transfer rate near the friction tool.

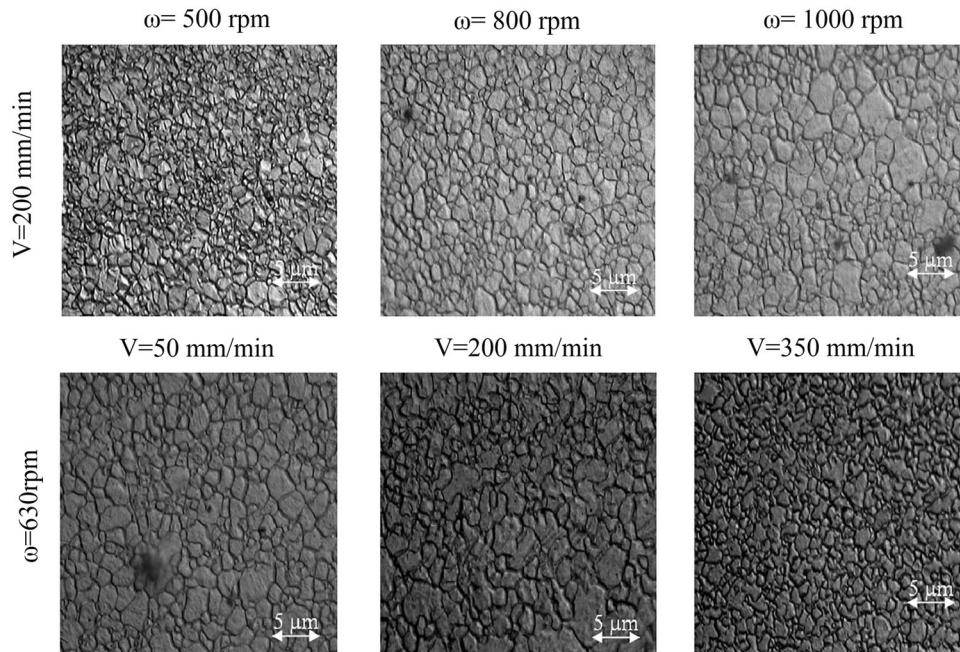
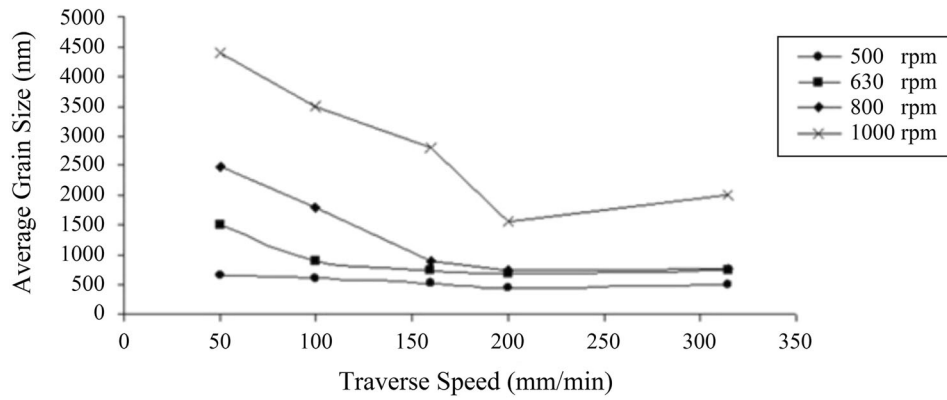


Fig. 7 Effect of rotational and traverse speed of friction tool on grain sizes in SFSP samples

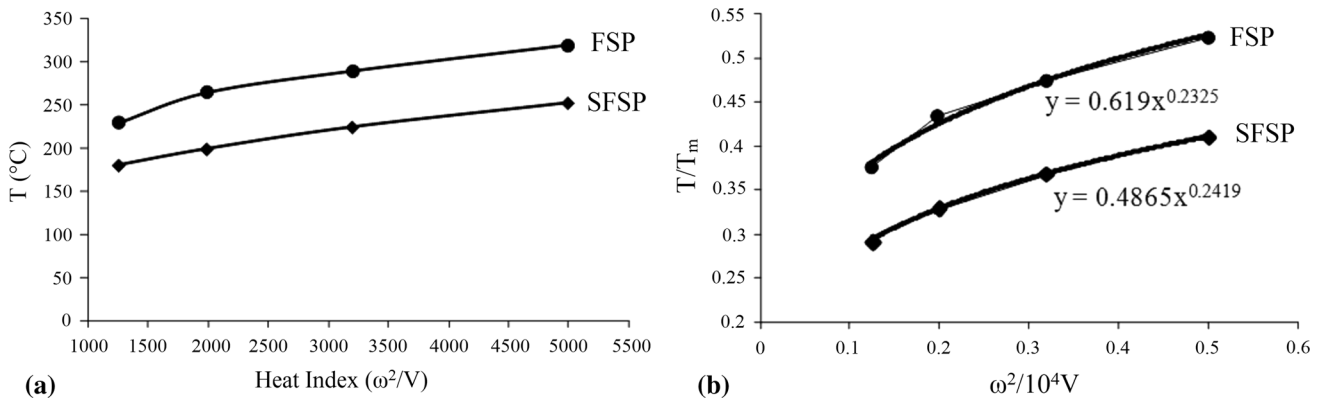


Fig. 8 (a) Variation of temperature and (b) variation of T/T_m ratio with the heat index in FSP and SFSP processes

$$T = 403 \left(\frac{\omega^2}{V \times 10^4} \right)^{0.2325} \quad (\text{Eq 3})$$

$$T = 316 \left(\frac{\omega^2}{V \times 10^4} \right)^{0.2419} \quad (\text{Eq 4})$$

3.3 Effects of Strain Rates

The rotating pin actuates the material flow during SFSP or FSP. The pin rotational speed determines the amount of material flow. Assuming that the rotation speed of the pin is about two times greater than the average flow rate of the

material, $\dot{\epsilon}$ during FSP can be expressed by the torsional deformation (Ref 25):

$$\dot{\epsilon} = \frac{R_m \cdot 2\pi r_e}{L_e} \quad (\text{Eq 5})$$

where $\dot{\epsilon}$, r_e , L_e , and R_m are the material flow strain rate, the effective radius, the depth of the dynamically recrystallized zone, and the average material flow rate, respectively.

The plastic flow of the materials in the dynamically recrystallized zone results in appearing an onion-like zone. An effective radius, r_e , that can represent the average radius for all parts of the materials inside the onion-like zone, is supposed to be 0.78 (or $\pi/4$) of the observed zone boundary radius (Ref 26-28). L_e can also be obtained the same way. In an applied ω of 630 rpm with $R_e \sim 2.34$ mm and $L_e \sim 5.3$ mm, $\dot{\epsilon}$ is calculated to be ~ 14.55 s⁻¹. Figure 9 reveals that applying the pin rotation speeds of 500-1000 rpm resulted in the strain rates within the range of 11.55-23.1 s⁻¹.

It seems that for constant rotation speed, an increase in tool traverse speed leads to a reduction in grain size, as shown in Fig. 7. The greater deformation of the material in higher traverse speeds can provide more strain-free sites for nucleation and reduce the grain size (Ref 29). According to Fig. 7, grain size gradually increases when traverse speed rises to more than 200 mm/min (see section 3.2). This observation is similar to the results obtained by Li et al. (Ref 30) in standard friction-stir-welded AZ31 joints. They found that the grains are coarsened if δ in Eq 2 is greater than 2.5, but on the contrary, the grains are refined if $\delta < 2.5$. This behavior attributed to the formation of voids, and they suggested further research to reveal the reasons for the void formation.

3.4 Texture Evaluation

Applying stresses greater than the critical resolved shear stress (CRSS) can activate four slip systems in magnesium materials, namely basal slip $\{0002\} < 11\bar{2}0 >$, prismatic slip $\{10\bar{1}0\} < 11\bar{2}0 >$, first-order pyramid slip $\{10\bar{1}1\} < 11\bar{2}0 >$ and second order pyramid slip $\{11\bar{2}2\} < 11\bar{2}3 >$ (Ref 8, 9). The temperature measurements in the stir zone demonstrated that it changed from 180 to 250 °C during SFSP, depending on the rotation and traverse speed of the tool. This indicates that temperature is high enough for activating the non-basal slip systems. However, introducing plastic deformation at a relatively high strain rate may restrict the activation of non-basal

slip systems in SFSPed materials, which results in activating only limited non-basal slip systems (Ref 28).

Figure 10 shows (0002), (10 $\bar{1}$ 0), and (10 $\bar{1}$ 1) pole figures of AZ31 Mg alloy sheet produced by hot rolling and SFSP in different rotation speeds. According to Fig. 10(a)-(d), the basal planes and prismatic planes of the SFSP samples were significantly different to that of base metal. Furthermore, Fig. 10 shows the trend of the prismatic and pyramidal slip in the stir zone to experience high strain rate deformation.

As seen in Fig. 11(a), increasing the rotation speed decreased the maximum value of (0002) pole intensity, while the maximum intensity values of (10 $\bar{1}$ 1) and (10 $\bar{1}$ 0) poles are increased. An increase in temperature during the SFSP process made some changes in the texture of the samples reducing the preferential texture intensity. Figure 11(b) illustrates that in constant rotational speed, the orientation of the texture changed with increasing the traverse speed. The relation between the intensity of the slip planes and traverse speed of the tool during SFSP (Fig. 11b) indicates that there is relatively no increase in the prismatic and pyramidal slips with increasing the traverse speed in the stir zone, while the intensity of the basal planes increases with increasing the traverse speed. It is concluded that promoting preferential texture is the result of increasing the rotational speed and decreasing the traverse speed.

3.5 Microhardness

In the case of the work-hardening alloys like AZ31, Jones et al. (Ref 31-33) reported two types of hardness profiles after FSP, which directly are related to working temperature, strain rate, and processing parameters. First, when grains growth or the amount of cold working decreases during FSP, the hardness of HAZ and TMAZ dramatically decreases compared with both base metal and nugget zones. Such profile is mainly observed in most 5xxx and 1xxx series of Al alloys. Second, in conditions that FSP produces fine grains, the hardness of SZ increases due to increase in high angle grain boundaries and existence of dislocation walls in some grains. This is more common in single-phase and low and medium stacking fault energy alloys like stainless steels and magnesium alloys. This profile is seen in SFSPed pieces.

In SZ, the hardness of AZ31 B alloy increases slightly with the decrease in grain size. The ultra-fine grains lead to pronounced microhardness change in the UFG zone of the FSP and SFSP specimens (Fig. 12). The highest hardness value (95 Hv) was even higher than those observed in the FSPed

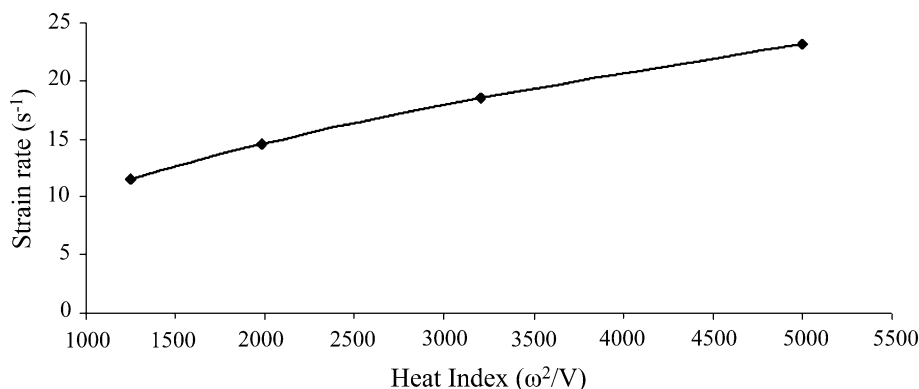


Fig. 9 The typical strain rates obtained for the pin rotation speeds of 500-1000 rpm

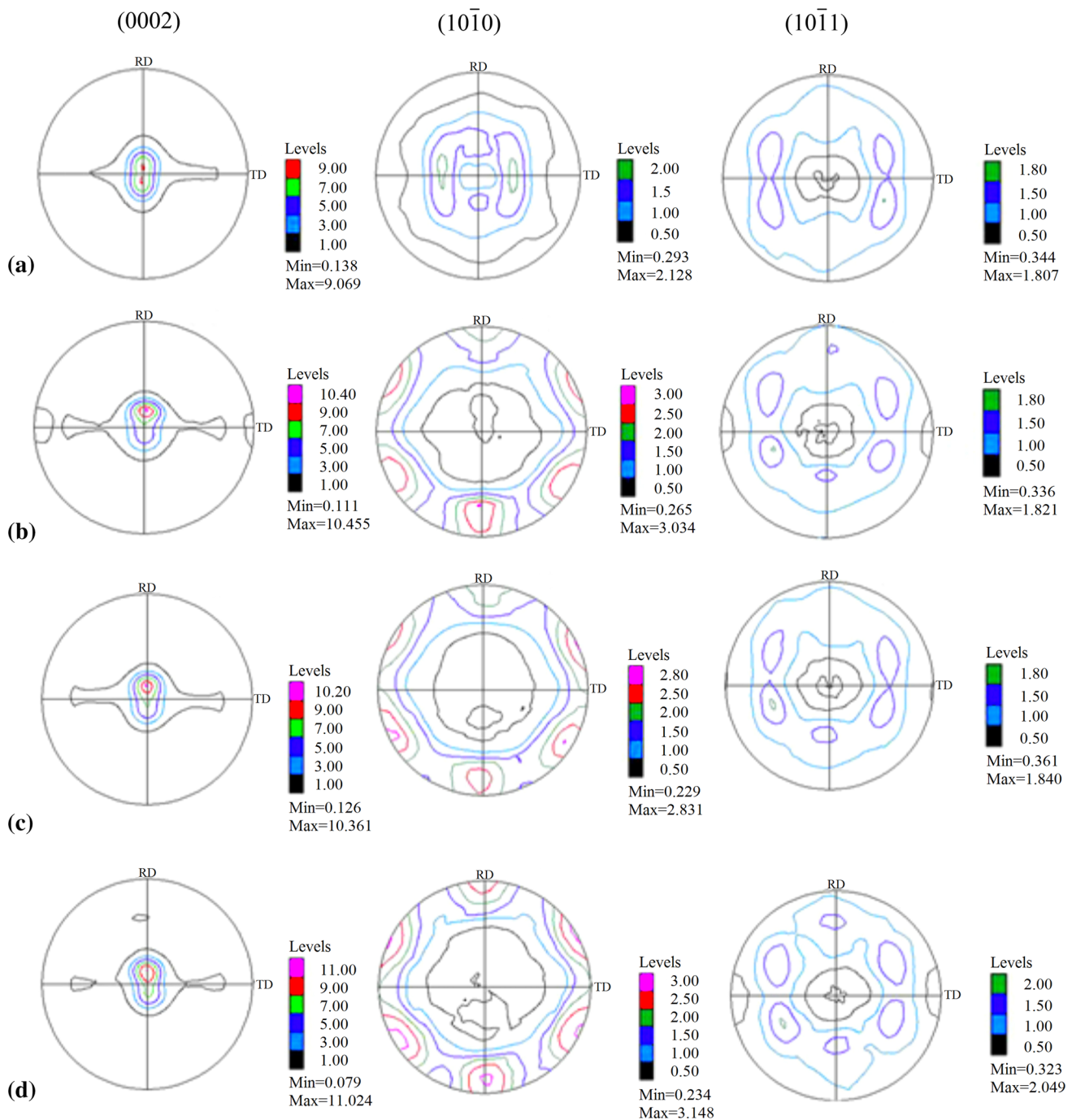


Fig. 10 The (0002), (10 $\bar{1}0$), and (10 $\bar{1}1$) complete pole figure of AZ31 Mg sheets processed by (a) hot rolling, and SFSP (b) 500 rpm, (c) 800 rpm and (d) 1000 rpm

AZ31. In the AZ31 B base metal, areas away from the nugget, the hardness remained around 45 Hv.

4. Conclusions

The solid solution-hardened AZ31 Mg alloy sheets were exposed to one-pass FSP and SFSP to investigate the effects of operation parameters on their microstructures and microhardness. The following results were obtained:

- (1) A uniform UFG microstructure can be achieved by proper control of the temperature profiles. The mean grain size was reduced to 400-900 nm by a single-pass SFSP compared to the initial value of 75 μm .
- (2) DDRX associated with distinct nucleation and growth stages was found to be responsible for the grain refinement.
- (3) The greater deformation of the material in higher traverse speeds provided more strain-free sites for nucleation and reduced the final grain size.

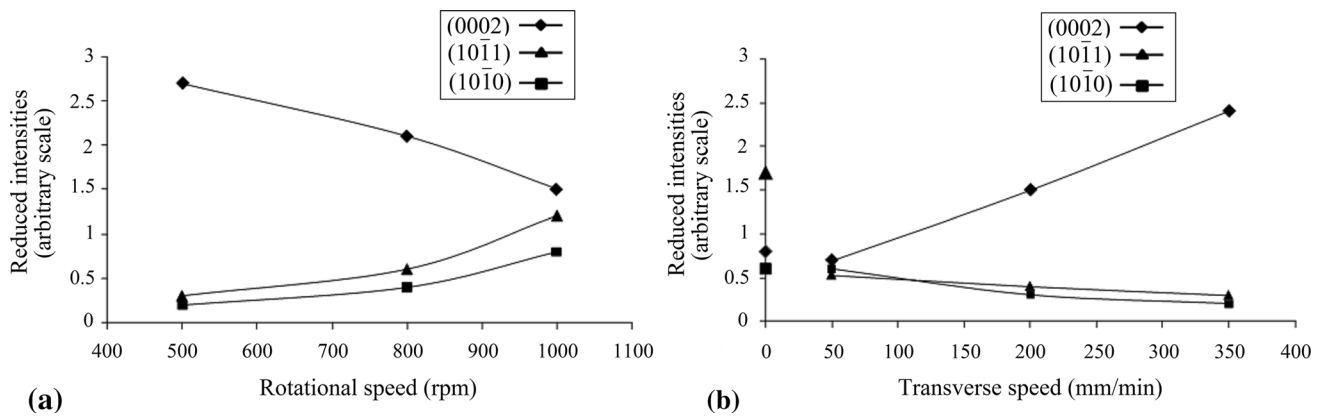


Fig. 11 The reduced intensities of the basal, prismatic and pyramidal reflection with the change of (a) rotational speed in traverse speed of 100 mm/min and (b) traverse speed in rotation speed of 1000 rpm

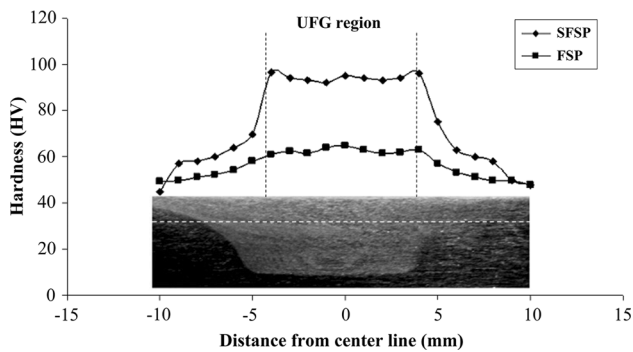


Fig. 12 Microhardness profile measured on cross-sectional planes for the FSPed and SFSPed AZ31 B alloy with the constant heat index ($\omega = 500$ rpm, $V = 200$ mm/min)

- (4) SFSP led to the variation of crystallographic orientation and enhancing the rotational speed and lowering the traverse speed promoted the development of a {0002} basal texture.
- (5) The UFG microstructure drastically increased the microhardness from an initial value of 45 to a final value of 90 Hv.

References

1. S.H. Chowdhury, D.L. Chen, S.D. Bhole, X. Cao, and P. Wanjara, Friction Stir Welded AZ31 Magnesium Alloy: Microstructure, Texture, and Tensile Properties, *Metall. Mater. Trans. A*, 2013, **44**(A), p 323–336
2. Y. Morisada, H. Fujii, T. Nagaoka, and M. Fukusumi, Nanocrystallized Magnesium Alloy—Uniform Dispersion of C60 Molecules, *Scr. Mater.*, 2006, **55**, p 1067–1070
3. C.J. Lee and J.C. Huang, High Strain Rate Super Plasticity of Mg Based Composites Fabricated by Friction Stir Processing, *Mater. Trans.*, 2006, **47**, p 2773–2778
4. T.A. Samman and G. Gottstein, Dynamic Recrystallization During High Temperature Deformation of Magnesium, *Mater. Sci. Eng. A*, 2008, **490**, p 411–420
5. J.Q. Su, T.W. Nelson, and C.J. Sterling, Friction Stir Processing of Large-Area Bulk UFG Aluminum Alloys, *Scr. Mater.*, 2005, **52**, p 135–140
6. H.S. Arewal, H.S. Singh, S. Singh, B.K. Dhindaw, D. McPhail, B. Shollock, R. Chater, and S. Mukherjee, Microstructure-Property Relationship for Friction Stir Processed Magnesium Alloy, *Adv. Eng. Mater.*, 2014, **16**(1), p 94–102
7. B. Mansoor and A.K. Ghosh, Microstructure and Tensile Behavior of a Friction Stir Processed Magnesium Alloy, *Acta Mater.*, 2012, **60**(13–14), p 5079–5088
8. C.W. Yang, Effect of Friction Stir Processing on the Microstructural Evolution and Tensile Behaviors of an α/β Dual-Phase Mg-Li-Al-Zn Alloy, *Mater. Trans.*, 2014, **55**(2), p 371–377
9. J. Chen, H. Fujii, Y. Sun, Y. Morisada, and R. Ueji, Fine Grained Mg-3Al-1Zn Alloy with Randomized Texture in the Double-Sided Friction Stir Welded Joints, *Mater. Sci. Eng. A*, 2013, **580**, p 83–91
10. R. Xin, D. Liu, B. Li, L. Sun, Z. Zhou, and Q. Liu, Mechanisms of Fracture and Inhomogeneous Deformation on Transverse Tensile Test of Friction-Stir-Processed AZ31 Mg Alloy, *Mater. Sci. Eng. A*, 2013, **565**, p 333–341
11. B.M. Darras, M.K. Khraisheh, F.K. Abu-Farha, and M.A. Omar, Friction Stir Processing of Commercial AZ31 Magnesium Alloy, *J. Mater. Process. Technol.*, 2007, **191**, p 77–81
12. C.I. Chang, X.H. Du, and J.C. Huang, Achieving Ultrafine Grain Size in Mg-Al-Zn Alloy by Friction Stir Processing, *Scr. Mater.*, 2007, **57**, p 209–212
13. H. Zhang and H. Liu, Characteristics and Formation Mechanisms of Welding Defects in Underwater Friction Stir Welded Aluminum Alloy, *Metall. Microsc. Anal.*, 2012, **1**, p 269–281
14. M.A. Wahid, Z.A. Khan, and A.N. Siddiquee, Review on Underwater Friction Stir Welding: A Variant of Friction Stir Welding with Great Potential of Improving Joint Properties, *Trans. Nonferrous Met. Soc. China*, 2018, **28**, p 193–219
15. N. Bhadouria, L. Thakur, P. Kumar, and N. Arora, An Investigation of Normal and Submerged Condition on Microstructural and Tribological Properties of Friction Stir Processed AZ91-D Magnesium Alloy, *Can. J. Metall. Mater. Sci., Can. Metall. Q.*, 2017, **56**, p 94–103
16. G. Cao and D. Zhang, Microstructure and Mechanical Properties of Submerged Friction Stir Processing Mg-Y-Nd Alloy, *Mater. Sci. Forum*, 2015, **816**, p 404–410
17. S. Benavides, Y. Li, L.E. Murr, D. Brown, and J.C. McClurr, Low-Temperature Friction-Stir Welding of 2024 Aluminum, *Scr. Mater.*, 1999, **41**, p 809–815
18. K.S. Wang, J.L. Wu, W. Wang, L.H. Zhou, Z.X. Lin, and L. Kong, Underwater Friction Stir Welding of Ultrafine Grained 2017 Aluminum Alloy, *J. Cent. South Univ.*, 2012, **19**(8), p 2081–2085
19. X. Feng, H. Liu, and J.C. Lippold, Microstructure Characterization of the Stir Zone of Submerged Friction Stir Processed Aluminum Alloy 2219, *Mater. Charact.*, 2013, **82**, p 97–102
20. M.A. Mofid, A. Abdollah-Zadeh, F. Malek Ghaini, and C. Hakan Gur, Submerged Friction-Stir Welding (SFSW) Underwater and Under Liquid Nitrogen: An Improved Method to Join Al Alloys to Mg Alloys, *Metall. Mater. Trans. A*, 2012, **43**(13), p 5106–5114
21. B. Darras and E. Kishta, Submerged Friction Stir Processing of AZ31 Magnesium Alloy, *Mater. Des.*, 2013, **47**, p 133–137

22. F. Chai, D. Zhang, and Y. Li, Microstructures and Tensile Properties of Submerged Friction Stir Processed AZ91 Magnesium Alloy, *J. Magn. Alloys*, 2015, **3**, p 203–209
23. G.K. Padhy, C.S. Wu, and S. Gao, Friction Stir Based Welding and Processing Technologies-Processes, Parameters, Microstructures and Applications: A Review, *Mater. Sci. Technol.*, 2018, **34**, p 1–38
24. M.J. Zehetbauer and Y.T. Zhu, Ed., *Bulk Nanostructured Materials*, Wiley, Weinheim, 2009
25. J.C. Huang, I.C. Hsiao, T.D. Wang, and B.Y. Lou, EBSD Study on Grain Boundary Characteristics in Fine-Grained Al Alloys, *Scr. Mater.*, 2000, **43**, p 213–217
26. A.J. Ardell, Precipitation Hardening, *Metall. Trans. A*, 1985, **16**, p 2131–2165
27. C.G. Rhodes, M.W. Mahoney, W.H. Bingel, and M. Calabrese, Fine-Grain Evolution in Friction-Stir Processed 7050 Aluminum, *Scr. Mater.*, 2003, **48**, p 1451–1455
28. Y.N. Wang, C.I. Chang, C.J. Lee, H.K. Lin, and J.C. Huang, Texture and Weak Grain Size Dependence in Friction Stir Processed Mg-Al-Zn Alloy, *Scr. Mater.*, 2006, **55**, p 637–640
29. S. Goel, G. Naveen, A. Gupta, and P. Gulati, Effect of Process Parameters on Mechanical and Metallurgical Properties of Friction Stir Processed AZ31 Mg Alloy, *Mater. Today Proc.*, 2018, **5**, p 4575–4583
30. W.Y. Li, T. Fu, L. Hütsch, J. Hilgert, F.F. Wang, J.F. dos Santos, and N. Huber, Effects of Tool Rotational and Welding Speed on Microstructure and Mechanical Properties of Bobbin-Tool Friction-Stir Welded Mg AZ31, *Mater. Des.*, 2014, **64**, p 714–720
31. Y.N. Wang and J.C. Huang, Transition of Dominant Diffusion Process During Superplastic Deformation in AZ61 Magnesium Alloys, *Metall. Mater. Trans. A*, 2002, **35**(2), p 555–562
32. C.I. Chang, C.J. Lee, and J.C. Hung, Relationship Between Grain Size and Zener–Holloman Parameter During Friction Stir Processing in AZ31 Mg Alloys, *Scr. Mater.*, 2004, **51**, p 509–514
33. M. Jones, P. Heurtier, C. Desrayaud, F. Montheillet, D. Allehaux, and J. Driver, Correlation Between Microstructure and Microhardness in a Friction Stir Welded 2024 Aluminium Alloy, *Scr. Mater.*, 2005, **52**, p 693–697

Publisher's Note Springer Nature remains neutral with regard to jurisdictional claims in published maps and institutional affiliations.